Three-Wave Interactions between Fast-Ion Modes in the National Spherical Torus Experiment

N. A. Crocker, W. A. Peebles, and S. Kubota
University of California, Los Angeles, California 90095-7099, USA

E. D. Fredrickson, S. M. Kaye, B. P. LeBlanc, and J. E. Menard
Princeton Plasma Physics Laboratory, Princeton, New Jersey 08543-0451, USA

(Received 18 August 2005; published 24 July 2006)

Simultaneous bursts of energetic particle mode (EPM) and toroidicity-induced Alfvén eigenmode (TAE) activity that correlate with significant fast-ion loss are observed in beam heated plasmas. Three-wave interactions between these modes are conclusively identified, indicating fixed phase relationships. This nonlinear coupling concentrates the energy of the TAEs into a toroidally localized perturbation frozen in the frame of a rigid, toroidally rotating structure formed by the EPMs. This redistribution of energy is significant because it will modify the effect of the TAEs on fast-ion loss.

DOI: 10.1103/PhysRevLett.97.045002 PACS numbers: 52.35.Mw, 52.35.Bj, 52.50.Gj, 52.55.Fa

The interaction of fast ions with plasma waves is a topic of significant interest in magnetic confinement fusion research, as well as in the study of the magnetosphere, ionosphere, and solar wind [1]. In fusion plasmas, fast ions are generated not only by heating techniques, such as neutral beam injection and ion cyclotron resonant frequency heating, but, in burning plasmas, they are also an inevitable byproduct of fusion reactions in the form of alpha particles. It is important that their energy be confined to the plasma. However, theoretical predictions and experimental observations demonstrate that these fast ions can excite global plasma perturbations, or fast-ion modes, that degrade their confinement by modifying orbits [2]. These modes also represent a potentially significant tool through which fast ions might be channeled to heat, drive current, and create internal transport barriers in fusion plasmas [3]. Understanding the dynamics of such modes is important in revealing, and possibly modifying, any deleterious effects on fast-ion confinement, as well as potentially enhancing beneficial effects such as fast-ion channeling. While much research has been performed on fast-ion modes, one area that has received little attention is the possible existence of nonlinear, three-wave interactions, or couplings, between the modes themselves. Such interactions, which require fixed phase relationships, can create coherent, or long-lived, structures. They can also transfer energy across disparate scales, potentially playing a significant role in mode damping, saturation, and excitation. The National Spherical Torus Experiment (NSTX) [4,5], where fast-ion modes are commonly observed [6], affords an opportunity to identify and study these interactions. We report here, for the first time, unambiguous identification of three-wave interactions between distinct fast-ion modes—toroidicity-induced Alfvén eigenmodes (TAEs) and energetic particle modes (EPMs) [6]—in neutral beam heated NSTX plasmas. Analysis shows that these interactions spatially concentrate the energy of the TAEs into a coherent, toroidally localized wave-packet whose envelope is frozen into a rigid, toroidally rotating structure formed by the EPMs. Previously, hints of similar interactions were reported on DIII-D [7], but clear identification was not made and their capacity to organize coherent structures not discussed.

In the results reported here, the interacting modes fall into two categories. One consists of a set of harmonics in frequency, f, and toroidal mode number, n, dominated by a low f ($\sim$25 kHz), low $n(=1)$ fundamental, that are EPMs of a type shown to be fishbones. The other consists of TAEs ($\sim$75–200 kHz), whose spectrum peaks around $f \sim$ 135 kHz and $n \sim 5$. Their frequencies and mode numbers increase in increments of $\Delta f \sim 25$ kHz and $\Delta n = 1$. Triplets of modes are identified whose frequencies and mode numbers, respectively, satisfy energy and momentum conservation laws (''selection rules'' or ''resonance conditions'' in [8]), suggesting that three-wave coupling occurs. This is confirmed through bicoherence analysis, which establishes unambiguously that the coupled modes have the requisite fixed phase relationships (''phase coherence'' or ''phase consistency'' in [8]). Further analysis reveals that the superposition of EPM harmonics forms a slowly evolving, toroidally rotating perturbation. It reveals, as well, that the three-wave interactions spatially concentrate the TAEs into a wave packet that is localized and frozen within the toroidal rotation frame of the EPM perturbation.

NSTX is a spherical torus with major and minor radii of $R = 0.85$ m and $a = 0.64$ m, respectively. For the results reported here, diverted L-mode helium plasmas are studied with toroidal plasma current and toroidal magnetic field of $I_p = 0.80$ MA and $B_T = 0.44$ T, respectively. In a typical discharge (shot 113546), I_p ramps up to a flattop in the first 250 ms of the discharge and then ramps back to zero between $t \approx 450$ and 600 ms [Fig. 1(a)]. Two 65 keV, 1 MW tangential deuterium neutral beams (with tangency major radii 0.592 and 0.487 m, respectively) are injected into the plasma from $t \approx$ 60–400 ms, for a total power of $P_{\mathrm{NB}} = 2$ MW [Fig. 1(a)]. Also, a high harmonic fast wave radio frequency heating power of $P_{\mathrm{rf}} = 2.5$ MW is applied from $t \approx$ 140–170 ms [Fig. 1(a)]. Multipoint Thomson

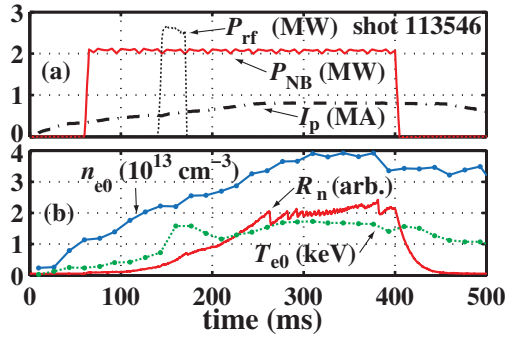

FIG. 1 (color online). Time histories of (a) toroidal plasma current, I_p, and power from neutral beams, P_{NB}, and high harmonic fast wave, P_{rf}; (b) central electron temperature and density, n_{e0} and T_{e0}, and D-D fusion neutron production rate, R_n.

scattering [9] shows that central electron temperature and density (T_{e0} and n_{e0}), respectively, rise to peak values of $\sim$1.7 keV and $\sim 3.85 \times 10^{19}$ m^{-3} at $\sim$300 ms, and then gradually decrease [Fig. 1(b)]. This peak density results in a central Alfvén velocity of $v_{A0} \sim 1.1 \times 10^6$ m/s, so the beam ions are $\sim$2.3 times Alfvénic in the plasma center. The beams create a fast deuterium (D) ion population in the plasma, which is signaled by a significant increase in the D-D fusion neutron rate, R_n [Fig. 1(b)]. There are many drops in the time period $t \sim 250$–400 ms that, as discussed below, correlate with bursts of mode activity. These drops indicate fast-ion loss [6]. The equilibrium modeling code, EFIT [5,10], constrained by external magnetic signals, indicates an elongation at the plasma boundary of $\kappa \sim 1.95$, and safety factors of $q(r) \sim 1$ for $r \lesssim 30$ cm and $q_{95} \sim 7$ at the 95% flux surface. It also indicates $\beta_N \sim 3.76$, $\beta_P \sim 0.74$, and $\beta_T \sim 10\%$. Modeling by the equilibrium transport code, TRANSP [11], indicates a central fast-ion beta, during the period of interest, $t = 350$–375 ms, of $\sim$13%. This takes into account the neutral beam sources, the EFIT equilibrium, and assumes neoclassical transport for the fast ions. Charge exchange recombination spectroscopy (CHERS) [12] shows a plasma toroidal rotation frequency, also during the period of interest, which is $\sim 30 \times 10^3$ rotations/s for $r \lesssim 20$ cm, falling off in a roughly linear fashion to zero at the plasma edge.

In NSTX, fast-ion modes are studied *locally* in the core plasma using reflectometry. A fixed-frequency, 50 GHz quadrature O-mode reflectometer launches microwaves into the plasma that reflect at the cutoff density of $\sim 3 \times 10^{19}$ m^{-3}. During the period of interest, the cutoff location is at $r \sim 25$ cm. Changes in the relative phase of the launched and reflected microwaves are measured and used to estimate density fluctuation levels at the cutoff via modeling [13]. Fast-ion modes are also studied at the plasma edge using an irregularly, toroidally distributed array of Mirnov coils outside the plasma that measure the time derivative of the poloidal magnetic field. For fast-ion modes that stand out from the turbulence, such as those discussed here, the array can resolve toroidal mode numbers up to $n = \pm 20$. Both the reflectometer and coil signals are recorded with sufficient bandwidth and resolution to easily resolve the fluctuations of interest, which have frequencies below $\sim$200 kHz.

The time-dependent spectra of reflectometer phase fluctuations [Fig. 2(b)] and magnetic fluctuations [Fig. 2(c)] show very similar, periodic bursts (every $\sim$2.5 ms) consisting of repeatable mode spectra between $t = 350$ and 370 ms. These bursts correlate with small drops in the neutron rate [Fig. 2(a)], indicating that they lead to loss of fast ions (note: neutron rate is low-pass filtered at $\sim$2 kHz). The lowest frequency mode typically reaches amplitudes of $\delta n/n_0 \sim 1.5\%$, determined via reflectometry, while the strongest mode in the range $\sim$75–200 kHz typically reaches amplitudes of $\sim$0.25%. (These fluctuation levels can be alternatively expressed as plasma, or density contour, displacements of $\xi_r \sim 6$ and 1 mm, respectively.) The strong similarity of the reflectometer phase and magnetic spectra establish that the observed modes are radially extended, or global, in character. The toroidal mode number of each mode is determined by examining the variation of its phase with toroidal position

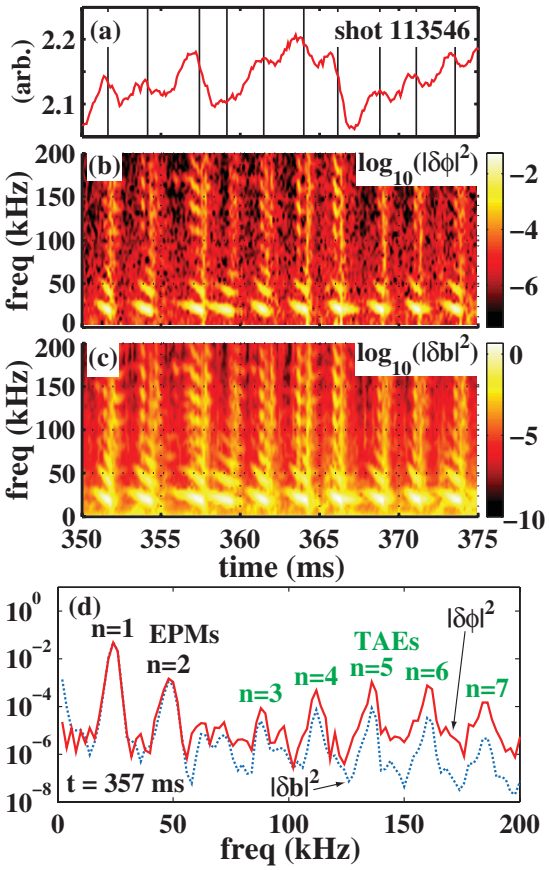

FIG. 2 (color). (a) Neutron rate vs time and time-dependent spectra of the (b) 50 GHz reflectometer phase and (c) edge magnetic fluctuations. Vertical lines in (a) mark bursts in (b) and (c). (d) Spectra from $t = 357.0$–357.5 ms with mode numbers determined from edge magnetics. EPMs ($n = 1, 2$) and TAEs ($n = 3$–7) are indicated.

using the coil array. Figure 2(d) shows spectra for both the reflectometer phase and magnetics for a typical burst ($t =$ 357.0–357.5 ms), indicating the mode numbers determined. The modes can be divided into two groups. Below 75 kHz, there is set of modes that are harmonics in f and n, consisting of a large amplitude ~25 kHz, $n = 1$ fundamental and a weaker ~50 kHz, $n = 2$ second harmonic. Their low mode numbers and frequencies combined with their bursting, rapid downward chirping character identifies them as EPMs of a type shown to be fishbones [6]. Above 75 kHz, there is a set of modes peaking at $n \sim 5$ and $f \sim 135$ kHz that have mode numbers $n = 3$–7 and frequencies increasing from $f \sim 85$ to 185 kHz in uniform increments of $\Delta f \sim 25$ kHz. Their frequencies and mode numbers combined with their bursting character indicate they are modes previously identified on NSTX as TAEs [6].

The frequency and mode number spacing between the TAEs suggests that they are three-wave coupled to the dominant ($n = 1$) EPM. First, the frequency spacing of adjacent TAEs is equal to the frequency of the dominant EPM, $f_{\mathrm{EPM}} \sim 25$ kHz. Second, the mode number spacing, $\Delta n = 1$, is equal to the mode number of the dominant EPM, $n_{\mathrm{EPM}} = 1$. These spacings indicate the existence of mode triplets that satisfy the three-wave energy and momentum matching conditions [8]. Specifically, adjacent pairs of TAEs, with frequencies f' and f'' and mode numbers n' and n'', satisfy the relationships $f'' = f_{\mathrm{EPM}} + f'$ and $n'' = n_{\mathrm{EPM}} + n'$. (A similar argument can be made for triplets consisting of the $n = 2$ EPM and pairs of TAEs satisfying the matching conditions.)

Confirmation of three-wave coupling is obtained by calculating the bicoherence of the reflectometer phase fluctuations (Fig. 3). Bicoherence is a standard statistical test for three-wave interactions [8]. For a measurement $x(t)$, the bicoherence (i.e., normalized bispectrum) b is defined in terms of its temporal Fourier components, $\hat{x}(f)$. The bispectrum is given by

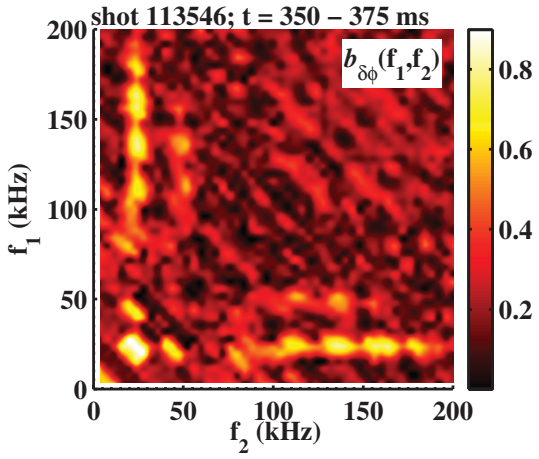

FIG. 3 (color). Bicoherence of 50 GHz reflectometer from $t =$ 350–375 ms. Maximum uncertainty is ~0.1.

$$B_x(f, f') = \langle \hat{x}(f)\hat{x}(f')\hat{x}^*(f + f') \rangle,$$

where $\langle \cdots \rangle$ denotes an average of multiple records. Bicoherence is then given by

$$b_x(f, f') = |B_x(f, f')| / (\langle |\hat{x}(f)\hat{x}(f')|^2 \rangle \langle |\hat{x}(f + f')|^2 \rangle)^{1/2}.$$

This definition has a particularly useful interpretation. When modes at frequencies f and f' interact with a mode at $f'' = f + f'$, they do so through the quadratic nonlinearity formed by their product. The bicoherence $b_x(f, f')$ is the coherence of the mode at f'' with this product. It can range from 0 to 1, with a higher value indicating a more statistically consistent interaction. A significant aspect of such consistency is that it requires a specific fixed phase relationship between the modes [8]: the total phase $\phi_x(f) + \phi_x(f') - \phi_x(f')$, where $\phi_x(f)$ is the phase of $\hat{x}(f)$, must be approximately the same for every record. If this does not hold true, the process of averaging over records to obtain the bispectrum will lead to destructive interference and reduction of the resulting bicoherence. The contour plot of bicoherence in Fig. 3 shows strong peaks in the bottom right and top left corners. Each peak corresponds to a triplet of modes whose frequencies and mode numbers, as discussed above, satisfy the matching requirements for three-wave interaction, thus confirming the interaction. (The strong peaks on the bottom left represent the various three-wave interactions between EPMs, which we do not discuss here.)

Further analysis of the EPMs and TAEs reveals that in each burst, the observed three-wave couplings organize the TAEs to spatially concentrate their energy into a toroidally localized wave packet. The envelope of this wave packet is stationary in the frame of a rigid, toroidally rotating perturbation formed by the superposition of the EPMs. The TAEs form a coherent structure because the uniform spacing of the components in the TAE spectrum, Δf_{TAE} and Δn_{TAE}, gives it a well-defined toroidal angular group velocity of $\varpi_{\mathrm{gTAE}} = 2\pi \Delta f_{\mathrm{TAE}} / \Delta n_{\mathrm{TAE}}$. The EPMs form a rigid, toroidally rotating perturbation because they are harmonics in f and n and thus have a common toroidal angular phase velocity of $\varpi_{\mathrm{EPM}} = 2\pi f_{\mathrm{EPM}} / n_{\mathrm{EPM}} \sim 2\pi(25\ \mathrm{kHz})/1$. This perturbation slowly evolves as the relative amplitudes of the EPMs change with time. Since, as noted above, $\Delta f_{\mathrm{TAE}} = f_{\mathrm{EPM}}$ and $\Delta n_{\mathrm{TAE}} = n_{\mathrm{EPM}}$, it follows that $\varpi_{\mathrm{gTAE}} = \varpi_{\mathrm{EPM}}$. Thus, the envelope of the coherent structure is frozen in the EPM frame. By appropriately filtering the reflectometer phase [e.g., with a 10 kHz bandpass for each mode in Fig. 2(d)] it is possible to isolate the contributions of both the EPM ($n = 1$–2) and TAE ($n = 3$–7) superpositions and, consequently, to see the structures they form propagate past the reflectometer (Fig. 4). From this analysis it can be seen that the three-wave interactions spatially concentrate the energy of the TAEs, forming a toroidally localized wave packet with, for instance, a full-width half-maximum toroidal extent of ~110° when the EPM perturbation peaks at $t \sim$ 357.4 ms. As expected, the wave packet maintains a fixed

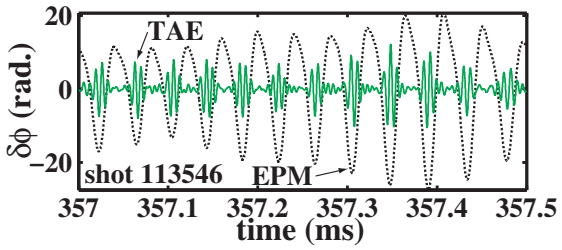

FIG. 4 (color online). The 50 GHz reflectometer phase filtered to show evolution of EPM perturbation and TAE wave packet around $t \sim 357$ ms.

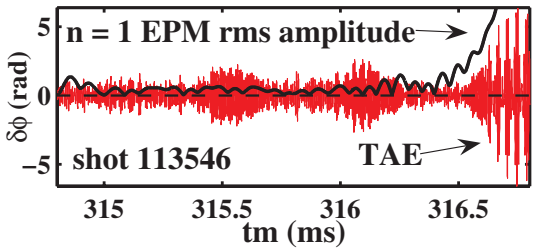

FIG. 5 (color online). The 50 GHz reflectometer phase around $t \sim 315$ ms filtered to show the TAE superposition and the amplitude of the $n = 1$ EPM.

position with respect to the EPM perturbation. This clearly indicates that three-wave interactions can substantially modify the perturbation formed by the TAEs. The resultant wave packet possesses a ''carrier wave,'' much shorter in wavelength than the dominant EPM, that propagates relative to the EPM perturbation. This is expected since the spectrum of the TAEs peaks at $(n, f) \sim (5, 135$ kHz), giving the carrier wave a toroidal angular phase velocity of $\varpi_{\mathrm{cTAE}} \sim 2\pi(135$ kHz$)/5$, which differs from ϖ_{EPM}.

It is important to note that when bursts of multiple TAEs are observed in the absence of the EPM, the superposition of the TAEs does not form a toroidally localized wave packet. This is illustrated in Fig. 5, which shows reflectometer phase from a period earlier in shot 113546 ($t \sim 315$ ms) that is filtered to isolate the TAE superposition (100–200 kHz) and the $n = 1$ EPM (10–27 kHz) amplitude. Two bursts of TAEs ($t \approx 315.5$ and 316.2 ms) precede a third TAE burst (starting at $t \approx 316.5$) that is accompanied by a burst of EPM activity. Unlike the first two bursts, the third clearly shows a strong, rapid modulation corresponding to the formation of a wave packet.

The results presented above motivate a simple physical model of the three-wave interactions between the EPMs and TAEs. The large amplitude ($\delta n/n_0 \gtrsim 1\%$) EPM perturbation, which is predominantly $n = 1$, clearly spatially modulates the medium in which the TAEs are excited and propagate. A resultant modulation of the free energy available to the TAEs—via, for example, modification of gradients—would then lead directly to the formation of the observed wave packet. Consistent with this, the modulation does, in fact, establish the necessary phase relationships between TAEs for the wave packet to form. This is reinforced by the observation that the wave packet is phase locked to the EPM rotation frame. The modulation may, of course, additionally play a role in nonlinearly exciting the TAEs that form the wave packet. This possibility, while interesting, is a topic for future investigation.

In summary, we conclusively identify three-wave interactions between energetic particle modes ($n = 1$–2, $f \lesssim 75$ kHz) and toroidicity-induced Alfvén eigenmodes ($n = 3$–7, $f \sim 75$–200 kHz, peaking around $f \sim 135$ kHz and $n \sim 5$). Triplets of modes, each consisting of a pair of TAEs and an EPM, satisfy the three-wave matching conditions for frequency and toroidal mode number and display high levels of bicoherence, conclusively establishing the existence of three-wave coupling. This nonlinear coupling spatially concentrates the TAE energy into a localized wave packet that is stationary in the EPM toroidal rotation frame. This spatial redistribution of the TAE mode energy is important because it will modify fast-ion orbits and, thereby, the fast-ion loss indicated by drops in neutron rate. Future comparison with nonlinear theory will improve overall understanding of the range of physical mechanisms at play, such as energy transfer between modes, and, thereby, allow us to more fully assess their effect on fast-ion confinement.

We wish to acknowledge T. Carter, B. Brugman, and T. Rhodes of the University of California, Los Angeles, as well as W. W. Heidbrink of University of California, Irvine, for useful discussions. We also wish to thank E. Ruskov of University of California, Irvine, for assistance with TRANSP modeling and R. E. Bell of Princeton Plasma Physics Laboratory for CHERS measurements. This work was supported by DOE Grant No. DE-FG02-99ER54527.

[1] C. Z. Cheng, J. Korean Phys. Soc. **31**, S127 (1997); L. Chen, *ibid.* **31**, S237 (1997).
[2] W. W. Heidbrink and G. J. Sadler, Nucl. Fusion **34**, 535 (1994); K. L. Wong, Plasma Phys. Controlled Fusion **41**, R1 (1999).
[3] K. L. Wong *et al.*, Phys. Rev. Lett. **93**, 085002 (2004).
[4] S. M. Kaye *et al.*, Fusion Technol. **36**, 16 (1999).
[5] S. A. Sabbagh *et al.*, Nucl. Fusion **41**, 1601 (2001).
[6] E. D. Fredrickson *et al.*, Phys. Plasmas **10**, 2852 (2003); E. Fredrickson, L. Chen, and R. White, Nucl. Fusion **43**, 1258 (2003); E. D. Fredrickson *et al.*, Europhys. Conf. Abstr. **29C**, P-1.061 (2005); E. D. Fredrickson *et al.*, Phys. Plasmas **13**, 056109 (2006).
[7] E. J. Strait, W. W. Heidbrink, and A. D. Turnbull, Plasma Phys. Controlled Fusion **36**, 1211 (1994).
[8] Y. C. Kim and E. J. Powers, Phys. Fluids **21**, 1452 (1978).
[9] B. P. LeBlanc, Rev. Sci. Instrum. **74**, 1659 (2003).
[10] L. L. Lao *et al.*, Nucl. Fusion **25**, 1611 (1985).
[11] J. P. H. E. Ongena, M. Evrard, and D. McCune, Fusion Technol. **33**, 181 (1998).
[12] D. Johnson and the NSTX Team, Plasma Phys. Controlled Fusion **45**, 1975 (2003).
[13] R. Nazikian, G. J. Kramer, and E. Valeo, Phys. Plasmas **8**, 1840 (2001).